

# Amplitude mode in a multi-gap superconductor $\text{MgB}_2$ investigated by terahertz two-dimensional coherent spectroscopy

Kota Katsumi,<sup>1,2,\*</sup> Jiahao Liang,<sup>1</sup> Ralph Romero III,<sup>1</sup> Ke Chen,<sup>3</sup> Xiaoxing Xi,<sup>3</sup> and N. P. Armitage<sup>1</sup>

<sup>1</sup>*William H. Miller III Department of Department of Physics and Astronomy,  
The Johns Hopkins University, Baltimore, Maryland 21218, USA*

<sup>2</sup>*Center for Quantum Phenomena, Department of Physics,  
New York University, New York, New York 10003, USA*

<sup>3</sup>*Department of Physics, Temple University, Philadelphia, Pennsylvania 19122, USA*

We have investigated terahertz (THz) nonlinear responses in a multi-gap superconductor,  $\text{MgB}_2$ , using THz two-dimensional coherent spectroscopy (THz 2DCS). With broad-band THz drives, we identified a well-defined nonlinear response near the lower superconducting gap energy  $2\Delta_\pi$  only at the lowest temperatures. Using narrow-band THz driving pulses, we observed first (FH) and third harmonic responses, and the FH intensity shows a monotonic increase with decreasing temperature when properly normalized by the driving field strength. This is distinct from the single-gap superconductor NbN, where the FH signal exhibited a resonant enhancement at temperatures near the superconducting transition temperature  $T_c$  when the superconducting gap energy was resonant with the driving photon energy and which had been interpreted to originate from the superconducting amplitude mode. Our results in  $\text{MgB}_2$  are consistent with a well-defined amplitude mode only at the lowest temperatures and indicate strong damping as temperature increases. This likely indicates the importance of interband coupling in  $\text{MgB}_2$  and its influence on the nature of the amplitude mode and its damping.

Multidimensional coherent spectroscopy gives new possibilities to acquire information about physical systems that other spectroscopies cannot [1]. Recently, it has been used in the terahertz (THz) frequency range, in the form of THz two-dimensional coherent spectroscopy (THz 2DCS) [2], to explore low-energy electrodynamics in various quantum materials, such as magnons [3–7], phonons [8, 9], plasmons [10–13], ferroelectric soft modes [14], electronic excitations in graphene [15],  $\text{LiNbO}_3$  [16], GaAs quantum wells [17], and electronic glasses [18]. In the case of a conventional superconductor NbN, we had demonstrated that the first-harmonic (FH) response of THz 2DCS is very sensitive to the amplitude mode of the superconducting (SC) order parameter via its paramagnetic light-matter coupling [19]. Among other aspects, it showed a resonant enhancement at temperatures near  $T_c$  when the SC gap energy was coincided with the THz driving photon energy.

THz 2DCS responses in a multi-gap superconductor are of particular interest, as it may host at least two amplitude modes and a relative phase mode of its order parameters, namely the Leggett mode [20–23]. To this aim,  $\text{MgB}_2$  is an ideal material which is known to be a  $s$ -wave multi-gap system [24]. THz nonlinear responses have been reported in  $\text{MgB}_2$  using pump-probe spectroscopy [25] or THz third-harmonic generations (THG) [26, 27]. Theoretical work has shown that in dirty-limit superconductors, the paramagnetic light-matter coupling plays a more crucial role in the THz nonlinear responses than the diamagnetic one, and the respective contributions of the amplitude modes, BCS quasiparticle excitations, and the Leggett mode depend on the level of disorder [28, 29]. It has also been pointed

out that the amplitude modes in multi-gap superconductors can exhibit marked differences compared to those in single-band counterparts due to the sensitivity to inter-band couplings [29]. Although the THz range nonlinearities have been investigated previously in multi-gap systems [30], the low-field limit where intrinsic superconducting properties are relevant was not emphasized.

To investigate the nature of the amplitude mode in a multi-gap superconductor, we performed THz 2DCS on a  $\text{MgB}_2$  thin film, with  $T_c = 38$  K. The details of the sample properties and the experimental setup are described in the Supplementary Material (SM) [31]. Using broad-band THz pulses, we identified a nonlinear response at the lower SC gap energy  $2\Delta_\pi$  at the lowest temperatures in the SC state. To further resolve the spectral features of the nonlinear response, we employed narrow-band THz pulses at the frequency of  $\Omega/2\pi = 0.63$  THz as the drives. Below  $T_c$ , we identified a nonlinear signal at the first harmonic (FH)  $\Omega$  and third-harmonic (TH)  $3\Omega$  frequencies. When the FH intensity is normalized by the THz field strength inside the film, it shows a monotonic increase with decreasing temperature. This is distinct from single-gap NbN where the normalized FH intensity is resonantly enhanced when twice the SC gap matches with  $\Omega$  [19]. We can fit the FH temperature dependence with a fitting model that assumes a damped-amplitude mode at  $\Omega = 2\Delta_\pi$ . Our results indicate that the essential difference in the amplitude mode between  $\text{MgB}_2$  and NbN, is most likely due to the effect of interband coupling, which modifies the line width of the amplitude mode in the  $\pi$  band.

To perform THz 2DCS, we generated two intense broad-band THz pulses by the tilted-pulse front tech-

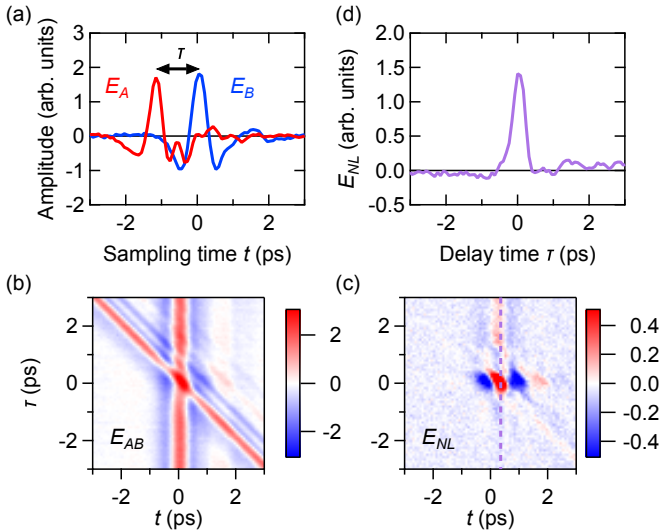


FIG. 1. (a) Time traces of the A and B pulses transmitted after the MgB<sub>2</sub> sample as a function of the sampling time  $t$ . The delay time between the A and B pulses is denoted as  $\tau$ . (b) 2D plot of the time traces of the A and B pulses together ( $E_{AB}(t, \tau)$ ) transmitted after the sample at 7 K as a function of  $t$  and  $\tau$ . (c) The nonlinear difference signal  $E_{NL}(t, \tau)$  from data in (b). (d) Time evolution of the nonlinear signal  $E_{NL}(t, \tau)$  as a function of  $\tau$  at a fixed sampling time  $t = 0$  ps, indicated by the vertical dashed line in (c).

nique with two LiNbO<sub>3</sub> crystals [32–34] (see SM for details). The time traces of the two THz pulses are measured by sweeping the timing between the sampling pulse and the THz pulses, as shown in Fig. 1(a). We swept the arrival time of the A-pulse with respect to that of the B-pulse to shift the delay time  $\tau$  between A and B pulses. We measured three sets of the transmitted THz electric fields ( $E$ -fields): only the A-pulse  $E_A(t, \tau)$ , only the B-pulse  $E_B(t)$ , and both pulses together  $E_{AB}(t, \tau)$ , which is shown in Fig. 1(b). Then, we obtain the nonlinear signal  $E$ -field as  $E_{NL}(t, \tau) = E_{AB}(t, \tau) - E_A(t, \tau) - E_B(t)$ , as shown in Fig. 1(c). It was essential that we set the peak  $E$ -fields of A and B pulses to 20 kV/cm to prevent the suppression of the SC state, which is confirmed by THz pump-THz probe spectroscopy (see SM). In the pump-probe experiments, the peak of the THz probe at 7 K in Fig. S3 displays a long-lived component, which has been ascribed to the quasiparticle excitations [25, 35]. On the contrary, the nonlinear signal  $E_{NL}(t = 0 \text{ ps}, \tau)$  in THz 2DCS is dominated by the response at  $\tau = 0$  ps, as shown in Fig. 1(d). This is the nonlinear signal inaccessible in pump-probe experiments but can be obtained by THz 2DCS, as discussed in Ref. [19].

In the upper panel of Fig. 2(a), we show the nonlinear drive fields at the sample position with no sample in place. In the lower panel of Fig. 2(a), we show the transmitted nonlinear intensity through the MgB<sub>2</sub> film. A peak is identified at 1 THz at 7K, which coincides

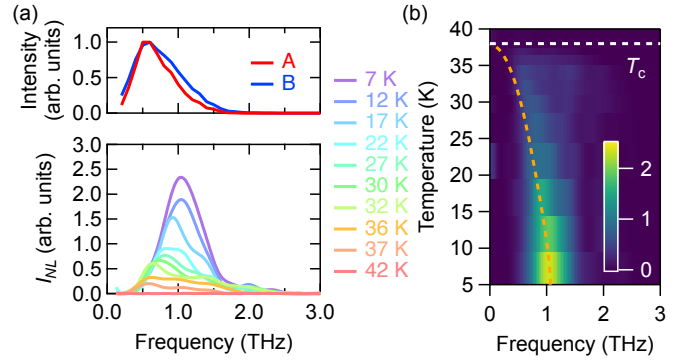


FIG. 2. (a) Top panel presents the power spectrum of the A and B pulses measured at the sample position with a GaP crystal. Bottom panel shows the power spectrum of the nonlinear signal at 7 K measured at  $\tau = 0$  ps with the broad-band THz pulses. (b) The power spectrum of the nonlinear signal as a function of temperature. The orange dashed curve is  $2\Delta_\pi$  computed by numerically solving the two-band BCS gap equations.

with the experimentally measured low temperature  $2\Delta_\pi$  value from linear optics. With increasing temperature, the nonlinear signal’s spectral weight displays a red shift, loses intensity, and broadens dramatically well below the SC transition temperature  $T_c$ . Figure 2(b) shows the temperature dependence of the nonlinear signal’s power spectra. The peak in the nonlinear signal initially follows the expected dependence for a mean-field two-gap model of  $2\Delta_\pi$  as shown by the orange dashed curve (See SM for further details), but is lost well before  $T_c$ . This comes from an intrinsic spectral property of the material because the peak position does not match the spectral maxima of the driving A and B pulse (shown in the top panel of Fig. 2(a)) nor the shape of the transmission spectra presented in Fig. S1(c) in SM. In the case of NbN, the red shift of the nonlinear signal’s peak at the SC gap energy was reported and attributed to the resonance of the amplitude mode of the SC order parameter [19]. However, in broad-band THz 2DCS experiments, multiple difference frequency components can contribute to four-wave mixing processes, complicating interpretation. Therefore, evaluating the precise amplitude and width of the peak can be difficult because the normalization of the nonlinear signal by the broad-band A and B pulses is challenging.

To further resolve the spectral features of the nonlinear signal, we performed THz 2DCS with a pair of narrow-band THz pulses, which significantly simplifies the four-wave mixing process and analysis. In Fig. 3(a), we show the power spectrum of the nonlinear signal from MgB<sub>2</sub> at 7 K using THz peak fields of 12 kV/cm when  $\tau = 0$  ps. The power spectrum exhibits two peaks at  $\Omega/2\pi = 0.63$  THz and  $3\Omega/2\pi = 1.9$  THz, corresponding to the fundamental (FH) and the third harmonic (TH) contributions, respectively. The FH and TH intensities

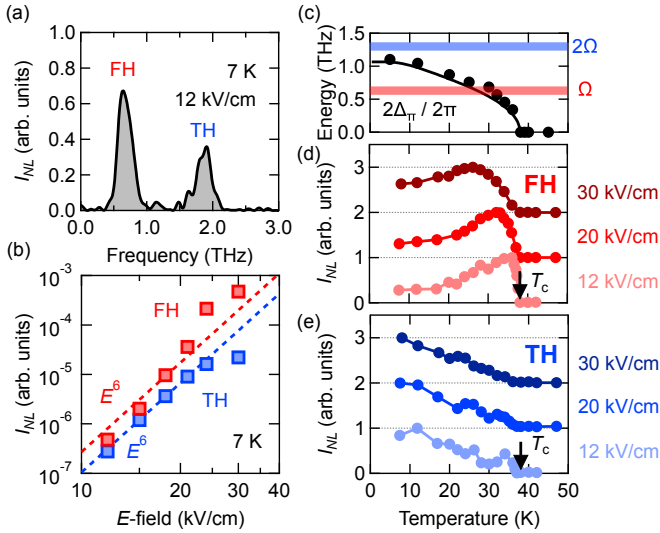


FIG. 3. (a) Power spectrum of the nonlinear signal at 7 K measured at  $\tau = 0$  ps with the narrow-band THz pulses. (b) The frequency-integrated intensity of the FH and TH contributions at 7 K when  $\tau = 0$  ps as a function of the B-pulse peak  $E$ -field in a log-log plot. Here, both A and B pulses are controlled equally. The dashed curves are the guides to the eye with a slope of 6. (c) Temperature dependence of the SC gap energies  $2\Delta_\pi$  evaluated from the equilibrium THz optical conductivity (circles). The solid curve is  $2\Delta_\pi$  computed by numerically solving the two-band BCS gap equations. (d) Raw data of the frequency-integrated intensity of the FH contribution as a function of temperature. The numbers on the right denote the peak  $E$ -field strength of the driving THz pulses. (e) The same plot as (c) but for the TH contribution.

follow  $E^6$  as shown in Fig. 3(b) up to 30 and 25 kV/cm, respectively, indicating that both are third-order nonlinear responses.

In Figs. 3(d) and (e), we plot the frequency-integrated intensity  $I_{NL}$  of the FH and TH signals as a function of temperature with the multi-cycle THz pulses when  $\tau = 0$  ps. Here, the nonlinear signal is integrated from 0.3 to 1 THz for the FH signal and from 1.6 to 2.2 THz for the TH signal. As shown in Fig. 3(d), for all measured THz  $E$ -fields, the FH signal displays a peak at a temperature below  $T_c$ , but note that unlike NbN it is not found at temperatures where the lower gap satisfies  $\Omega = 2\Delta_\pi$  (Fig. 3(c)). Moreover, when we increase the THz  $E$ -field strength, the peak temperature decreases as superconductivity is suppressed. This highlights the importance of using small drive fields to measure the intrinsic superconducting properties. The temperature evolution of the TH signal agrees well with the previous THG experiments, where it takes its maximum toward  $2\Omega = 2\Delta_\pi$  [26].

In order to consider the actual temperature dependence of any resonant features, one must take into account the screening effect on the internal THz  $E$ -field. As presented in Fig. S4(a) in SM, the transmitted A

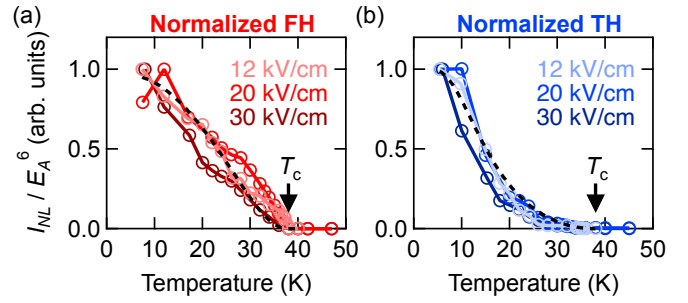


FIG. 4. Temperature dependence of the frequency-integrated intensity of the (a) FH and (b) TH contributions normalized by the transmitted  $E$ -field of the A-pulse. Black dashed curves are the fits using Eq. (1) with  $\omega = \Omega$  for the FH and  $\omega = 2\Omega$  for the TH signals.

and B fields from the sample decrease when the temperature is lowered below  $T_c$ . Following the procedure in Ref. [19], we normalize the FH and TH intensities by the sixth power of the transmitted  $E$ -field of the A-pulse, as shown in Fig. 4. While the behavior of the TH signal is unchanged by the normalization, surprisingly, the FH signal shows a monotonic increase when the temperature is decreased for all the driving THz  $E$ -fields studied here. This is in stark contrast to the result of NbN, whose normalized FH signal exhibits a resonant enhancement when the driving frequency  $\Omega$  matches the SC gap  $2\Delta$  [19]. The same result qualitatively is obtained when the B-pulse is used for normalization (see SM). We stress that one must properly normalize the intensity of the nonlinear response to obtain its correct temperature dependence, as pointed out in previous THG [36, 37] and THz 2DCS experiments [19].

This result indicates that the nature of the FH signal in MgB<sub>2</sub> is distinct from that in NbN, even though their linear responses are similar [19]. In Ref. [19], it was shown that the FH nonlinear response in NbN is dominated by the amplitude mode for a wide range of impurity levels  $3 \leq k_F l \leq 30$ , where  $k_F$  is the Fermi wave vector and  $l$  is the electronic mean free path. In the case of our MgB<sub>2</sub> films, the zero-frequency resistivity is estimated as  $50 \mu\Omega$  cm, and  $k_F l$  is estimated as approximately 13.5 [38, 39]. Therefore, the FH nonlinear signal is most likely dominated by the amplitude modes. The difference in the amplitude modes in single and multi-gap superconductors was theoretically examined in Ref. [29], and it was found that the respective ratio of the two amplitude modes significantly changes if the interband coupling strength is finite. For the parameters assumed in MgB<sub>2</sub>, the amplitude mode of the  $\pi$  band was strongly suppressed, and that of the  $\sigma$  band is pronounced. Nevertheless, we did not observe the resonance when the higher SC gap energy  $2\Delta_\sigma$  matched with  $\Omega$ . This is presumably because the calculation assumes zero-temperature, while the temperature satisfying  $\Omega = 2\Delta_\sigma$  is just below  $T_c$ , and

the damping is more significant at such a high temperature.

To quantitatively examine the interpretation above, we evaluated the temperature dependence of the FH and TH nonlinear signals by fitting them with a model for the amplitude-mode resonance developed in Ref. [19]:

$$I(\omega, T) = I_0 \frac{\Delta_\pi(T)^2}{(\omega + i\delta)^2 - (2\Delta_\pi(T))^2}. \quad (1)$$

Here,  $\omega$  is the angular frequency,  $T$  is the temperature,  $\delta$  is the scattering rate of the resonance, and  $I_0$  is a constant. Given the fact that the broad-band nonlinear signal displays the peak at  $2\Delta_\pi$  at the lowest temperature, we set the resonant condition in the same manner as NbN, i.e.,  $\omega = \Omega$  for the FH and  $\omega = 2\Omega$  for the TH. For the driving field strength of 12 kV/cm, the FH and TH can be simultaneously fit with  $\delta = 0.55$  THz. This obtained  $\delta$  is much larger than  $\delta = 0.12$  THz in NbN [19]. This result is consistent with the interpretation that the resonance at  $\Omega = 2\Delta_\pi$  in MgB<sub>2</sub> is strongly damped due to the interband coupling near the inferred resonance temperature. It could also be because the temperature where the resonance condition would be met is approximately two times higher in MgB<sub>2</sub>.

In summary, we performed THz 2DCS on the multi-gap superconductor MgB<sub>2</sub>. Utilizing broad-band THz pulses, we observed a nonlinear signal peaked at the lower SC gap energy  $2\Delta_\pi$  at our lowest measured temperatures. The signal rapidly decays with increasing temperature. With narrow-band THz pulses, a nonlinear signal is found at the FH and TH of the driving THz frequency  $\Omega$ . The normalized FH signal displays a monotonic increase with lowering the temperature, unlike the resonant enhancement found near  $T_c$  at  $\Omega = 2\Delta$  reported in NbN. This is consistent with a much larger damping rate of the amplitude mode in MgB<sub>2</sub>, at least in the temperature range of interest where the resonant condition is met. Our observations demonstrate the difference in the SC amplitude mode in MgB<sub>2</sub> and NbN, and likely highlight the importance of the interband couplings in the SC collective excitations.

We thank L. Benfatto, J. Fiore, M. Udina, and G. Seibold for fruitful discussions. This project was supported by the Gordon and Betty Moore Foundation, EPiQS initiative, Grant No. GBMF-9454 and NSF-DMR 2226666. K.K. was supported by the Overseas Research Fellowship of the JSPS. K.C. and X.X. were supported by the U.S. Department of Energy, Office of Science under Grant DE-SC0022330.

---

\* kota.katsumi@nyu.edu

[1] S. T. Cundiff and S. Mukamel, *Physics Today* **66**, 44 (2013).

- [2] M. Woerner, W. Kuehn, P. Bowlan, K. Reimann, and T. Elsaesser, *New J. Phys.* **15**, 025039 (2013).
- [3] J. Lu, X. Li, H. Y. Hwang, B. K. Ofori-Okai, T. Kurihara, T. Suemoto, and K. A. Nelson, *Phys. Rev. Lett.* **118**, 207204 (2017).
- [4] E. A. Mashkovich, K. A. Grishunin, R. M. Dubrovin, A. K. Zvezdin, R. V. Pisarev, and A. V. Kimel, *Science* **374**, 1608 (2021).
- [5] T. G. H. Blank, K. A. Grishunin, B. A. Ivanov, E. A. Mashkovich, D. Afanasiev, and A. V. Kimel, *Phys. Rev. Lett.* **131**, 096701 (2023).
- [6] Z. Zhang, F. Y. Gao, J. B. Curtis, Z.-J. Liu, Y.-C. Chien, A. von Hoegen, M. T. Wong, T. Kurihara, T. Suemoto, P. Narang, *et al.*, *Nature Physics*, 1 (2024).
- [7] Z. Zhang, F. Y. Gao, Y.-C. Chien, Z.-J. Liu, J. B. Curtis, E. R. Sung, X. Ma, W. Ren, S. Cao, P. Narang, *et al.*, *Nature Physics*, 1 (2024).
- [8] G. Folpini, K. Reimann, M. Woerner, T. Elsaesser, J. Hoja, and A. Tkatchenko, *Phys. Rev. Lett.* **119**, 097404 (2017).
- [9] T. G. H. Blank, K. A. Grishunin, K. A. Zvezdin, N. T. Hai, J. C. Wu, S.-H. Su, J.-C. A. Huang, A. K. Zvezdin, and A. V. Kimel, *Phys. Rev. Lett.* **131**, 026902 (2023).
- [10] S. Houver, L. Huber, M. Savoini, E. Abreu, and S. L. Johnson, *Opt. Express* **27**, 10854 (2019).
- [11] A. Liu, D. Pavicevic, M. H. Michael, A. G. Salvador, P. E. Dolgirev, M. Fechner, A. S. Disa, P. M. Lozano, Q. Li, G. D. Gu, E. Demler, and A. Cavalleri, arXiv:2308.14849 (2023).
- [12] A. Gómez Salvador, P. E. Dolgirev, M. H. Michael, A. Liu, D. Pavicevic, M. Fechner, A. Cavalleri, and E. Demler, *Phys. Rev. B* **110**, 094514 (2024).
- [13] N. Taherian Hosseinabadi, M. Först, A. Liu, M. Fechner, D. Pavicevic, A. von Hoegen, E. Rowe, Y. Liu, S. Nakata, B. Keimer, *et al.*, arXiv preprint arXiv:2401.01115 (2024).
- [14] S. Pal, N. Strkalj, C.-J. Yang, M. C. Weber, M. Trassin, M. Woerner, and M. Fiebig, *Phys. Rev. X* **11**, 021023 (2021).
- [15] P. Bowlan, E. Martinez-Moreno, K. Reimann, T. Elsaesser, and M. Woerner, *Phys. Rev. B* **89** (2014).
- [16] C. Somma, K. Reimann, C. Flytzanis, T. Elsaesser, and M. Woerner, *Phys. Rev. Lett.* **112**, 146602 (2014).
- [17] T. Maag, A. Bayer, S. Baierl, M. Hohenleutner, T. Korn, C. Schüller, D. Schuh, D. Bougeard, C. Lange, R. Huber, *et al.*, *Nat. Phys.* **12**, 119 (2016).
- [18] F. Mahmood, D. Chaudhuri, S. Gopalakrishnan, R. Nandkishore, and N. P. Armitage, *Nat. Phys.* **17**, 627–631 (2021).
- [19] K. Katsumi, J. Fiore, M. Udina, R. Romero, D. Barbalas, J. Jesudasan, P. Raychaudhuri, G. Seibold, L. Benfatto, and N. P. Armitage, *Phys. Rev. Lett.* **132**, 256903 (2024).
- [20] A. Leggett, *Progress of Theoretical Physics* **36**, 901 (1966).
- [21] G. Blumberg, A. Mialitsin, B. S. Dennis, M. V. Klein, N. D. Zhigadlo, and J. Karpinski, *Phys. Rev. Lett.* **99**, 227002 (2007).
- [22] M. V. Klein, *Phys. Rev. B* **82**, 014507 (2010).
- [23] T. Cea and L. Benfatto, *Phys. Rev. B* **94**, 064512 (2016).
- [24] X. Xi, *Reports on Progress in Physics* **71**, 116501 (2008).
- [25] F. Giorgianni, T. Cea, C. Vicario, C. P. Hauri, W. K. Withanage, X. Xi, and L. Benfatto, *Nat. Phys.* **15**, 341 (2019).
- [26] S. Kovalev, T. Dong, L.-Y. Shi, C. Reinhofer, T.-Q. Xu,

- H.-Z. Wang, Y. Wang, Z.-Z. Gan, S. Germanskiy, J.-C. Deinert, I. Ilyakov, P. H. M. van Loosdrecht, D. Wu, N.-L. Wang, J. Demsar, and Z. Wang, *Phys. Rev. B* **104**, L140505 (2021).
- [27] C. Reinthoffer, P. Pilch, A. Reinold, P. Derendorf, S. Kovalev, J.-C. Deinert, I. Ilyakov, A. Ponomaryov, M. Chen, T.-Q. Xu, Y. Wang, Z.-Z. Gan, D.-S. Wu, J.-L. Luo, S. Germanskiy, E. A. Mashkovich, P. H. M. van Loosdrecht, I. M. Eremin, and Z. Wang, *Phys. Rev. B* **106**, 214514 (2022).
- [28] Y. Murotani and R. Shimano, *Phys. Rev. B* **99**, 224510 (2019).
- [29] J. Fiore, M. Udina, M. Marciari, G. Seibold, and L. Benfatto, *Phys. Rev. B* **106**, 094515 (2022).
- [30] L. Luo, M. Mootz, J. H. Kang, C. Huang, K. Eom, J. W. Lee, C. Vaswani, Y. G. Collantes, E. E. Hellstrom, I. E. Perakis, C. B. Eom, and J. Wang, *Nat. Phys.* **19**, 201 (2023).
- [31] See Supplemental Material for the details of the equilibrium optical properties of the sample, experimental setup, and the additional data, which includes [36, 40–44].
- [32] J. Hebling, G. Almasi, I. Kozma, and J. Kuhl, *Opt. Express* **10**, 1161 (2002).
- [33] S. Watanabe, N. Minami, and R. Shimano, *Opt. Express* **19**, 1528 (2011).
- [34] H. Hirori, A. Doi, F. Blanchard, and K. Tanaka, *Appl. Phys. Lett.* **98**, 091106 (2011).
- [35] J. Demsar, R. D. Averitt, A. J. Taylor, V. V. Kabanov, W. N. Kang, H. J. Kim, E. M. Choi, and S. I. Lee, *Phys. Rev. Lett.* **91**, 267002 (2003).
- [36] K. Katsumi, M. Nishida, S. Kaiser, S. Miyasaka, S. Tajima, and R. Shimano, *Phys. Rev. B* **107**, 214506 (2023).
- [37] H. Chu, M.-J. Kim, K. Katsumi, S. Kovalev, R. D. Dawson, L. Schwarz, N. Yoshikawa, G. Kim, D. Putzky, Z. Z. Li, H. Raffy, S. Germanskiy, J.-C. Deinert, N. Awari, I. Ilyakov, B. Green, M. Chen, M. Bawatna, G. Cristiani, G. Logvenov, Y. Gallais, A. V. Boris, B. Keimer, A. P. Schnyder, D. Manske, M. Gensch, Z. Wang, R. Shimano, and S. Kaiser, *Nat. Commun.* **11**, 1793 (2020).
- [38] A. V. Sologubenko, J. Jun, S. M. Kazakov, J. Karpinski, and H. R. Ott, *Phys. Rev. B* **66**, 014504 (2002).
- [39] R. Lal, A. Vajpayee, V. Awana, H. Kishan, and A. Awasthi, *Physica C: Superconductivity* **469**, 106 (2009).
- [40] D. C. Mattis and J. Bardeen, *Phys. Rev.* **111**, 412 (1958).
- [41] W. Zimmermann, E. Brandt, M. Bauer, E. Seider, and L. Genzel, *Physica C: Superconductivity* **183**, 99 (1991).
- [42] X. Xi, A. Pogrebnikov, S. Xu, K. Chen, Y. Cui, E. Maertz, C. Zhuang, Q. Li, D. Lamborn, J. Redwing, Z. Liu, A. Soukiassian, D. Schlom, X. Weng, E. Dickey, Y. Chen, W. Tian, X. Pan, S. Cybart, and R. Dynes, *Physica C: Superconductivity* **456**, 22 (2007).
- [43] R. A. Kaindl, M. A. Carnahan, J. Orenstein, D. S. Chemla, H. M. Christen, H.-Y. Zhai, M. Paranthaman, and D. H. Lowndes, *Phys. Rev. Lett.* **88**, 027003 (2001).
- [44] K. Isoyama, N. Yoshikawa, K. Katsumi, J. Wong, N. Shikama, Y. Sakishita, F. Nabeshima, A. Maeda, and R. Shimano, *Commun. Phys.* **4**, 160 (2021).

# Amplitude mode in a multi-gap superconductor MgB<sub>2</sub> investigated by terahertz two-dimensional coherent spectroscopy

## Supplemental Material

Kota Katsumi,<sup>1,2,\*</sup> Jiahao Liang,<sup>1</sup> Ralph Romero III,<sup>1</sup> Ke Chen,<sup>3</sup> Xiaoxing Xi,<sup>3</sup> and N. P. Armitage<sup>1</sup>

<sup>1</sup>*William H. Miller III Department of Department of Physics and Astronomy,  
The Johns Hopkins University, Baltimore, Maryland 21218, USA*

<sup>2</sup>*Center for Quantum Phenomena, Department of Physics,  
New York University, New York, New York 10003, USA*

<sup>3</sup>*Department of Physics, Temple University, Philadelphia, Pennsylvania 19122, USA*

### I. SAMPLE DETAILS

High-quality 20 nm-thick MgB<sub>2</sub> films were grown on a single-crystal MgO (111) substrate by hybrid physical-chemical vapor deposition (HPCVD) [1]. The details of the sample fabrication are documented in Refs. [1, 2].

We evaluated the lower superconducting (SC) gap of the MgB<sub>2</sub> sample by terahertz (THz) time-domain spectroscopy. The obtained optical conductivity  $\sigma(\omega)$  is presented in Fig. S1. In its real part at 5 K, the opening of twice the lower gap  $2\Delta_\pi$  is identified around 1 THz. We evaluated twice the SC gap  $2\Delta_\pi$  at different temperatures by the two-components Mattis-Bardeen (MB) model [3–5]. Here, we set the parameters as summarized in Table 1, similar to the values in Ref. [5]. The values of twice the higher gap  $2\Delta_\sigma$  are adopted from the solutions of the BCS gap equations for two bands as described in the next section.

We plot the obtained  $2\Delta_\pi$  as a function of temperature in Fig. S2 by the red circles. It follows the solutions for  $2\Delta_\pi$  of the BCS gap equations and is consistent with the previous THz experiments [6, 7] and scanning tunneling microscopy (STM) [8].

TABLE I. Parameters for the MB model for each band.  $2\Delta(T=0\text{ K})$ ,  $\omega_p$ , and  $\tau_p$  denote twice the SC gap energy at  $T=0\text{ K}$ , plasma frequency, and the scattering rate, respectively.  $\omega_p$  and  $\tau_p$  are kept fixed through all the temperatures.

	$2\Delta(T=0\text{ K})/2\pi$ (THz)	$\omega_p$ (eV)	$1/\tau_p$ (meV)
$\pi$ band	1.1	5.2	12.5
$\sigma$ band	3.4	4.2	8.33

### II. EVALUATING THE SC GAP ENERGIES

We evaluated the temperature dependence of the SC gap energies  $2\Delta_\pi$  and  $2\Delta_\sigma$  by self-consistently solving

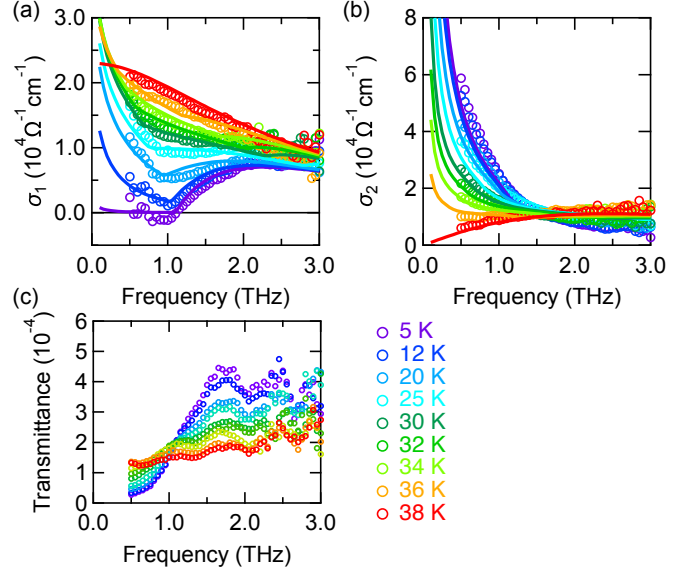


FIG. S1. (a) Real and (b) imaginary parts of the optical conductivity of MgB<sub>2</sub> ( $T_c = 38\text{ K}$ ). The solid curves are the optical conductivity calculated by the two-components MB model. (c) THz power transmittance as a function of temperature.

the BCS gap equations for two bands [2, 9]:

$$\Delta_\alpha = \sum_{\beta=\pi,\sigma} V_{\alpha\beta} \Delta_\beta F(\Delta_\beta), \quad (\text{S1})$$

where  $F(\Delta_\beta)$  is defined as

$$F(\Delta_\beta) = N_\beta \int_0^{\omega_c} d\xi \frac{\tanh(\sqrt{\xi^2 + \Delta_\beta^2}/2k_B T)}{\sqrt{\xi^2 + \Delta_\beta^2}}. \quad (\text{S2})$$

Here,  $\Delta_\beta$  and  $N_\beta$  are the SC gap energy and the density of states at the Fermi energy of the  $\beta$ -th band ( $\beta = \pi, \sigma$ ), respectively.  $V_{\alpha\beta}$  are the matrix elements of the interaction, which determine the intraband ( $\alpha = \beta$ ) and interband ( $\alpha \neq \beta$ ) coupling constants,  $\omega_c$  is the cut-off frequency,  $k_B$  is the Boltzmann constant,  $T$  is the temperature. For the case of MgB<sub>2</sub>, the following dimensionless parameters are believed to describe the SC gap

\* kota.katsumi@nyu.edu

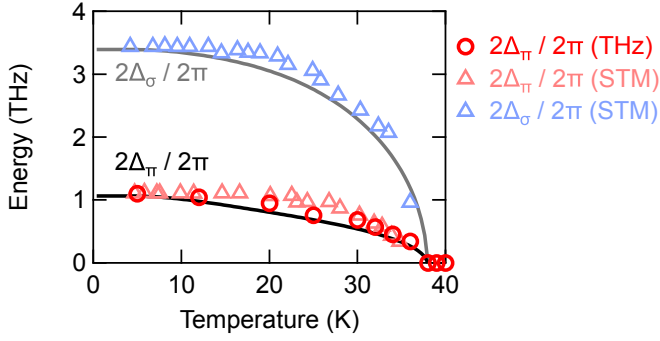


FIG. S2. (a) Temperature dependence of the SC gap energy of  $\pi$  and  $\sigma$  bands of  $\text{MgB}_2$ . Red circles show  $2\Delta_\pi$  evaluated by THz time-domain spectroscopy in equilibrium. Red and blue triangles are values of  $2\Delta_\pi$  and  $2\Delta_\sigma$  adopted from the previous STM experiments [8]. The solid black and gray curves are the solutions of the BCS gap equations.

well [10]:  $\lambda_{11} = V_{11}N_1 = 0.28$ ,  $\lambda_{22} = V_{22}N_2 = 0.96$ , and  $\lambda_{12} = \lambda_{21} = V_{12}\sqrt{N_1N_2} = 0.19$ , and  $N_2/N_1 = 0.73$ . We adopted the cut-off frequency as  $\omega_c = 1.78$  THz from the literature [11].

We can solve Eqs. (S1) for the  $\pi$  and  $\sigma$  bands self-consistently, and the obtained SC gap energies are presented in Fig. S2 by the solid curves. The curves show good agreement with the experimental data of  $2\Delta_\pi$  in our THz experiments (the red circles) and the STM ( $2\Delta_\pi$  and  $2\Delta_\sigma$  by the red and blue triangles, respectively).

### III. EXPERIMENTAL DETAILS

To perform THz two-dimensional coherent spectroscopy (2DCS), we utilized a regenerative amplified Ti:sapphire laser with a center wavelength of 800 nm, pulse duration of 100 fs, pulse energy of 9 mJ, and repetition rate of 1 kHz. We divided the output from the regenerative amplifier into three beams: two for generating intense THz pulses (A and B pulses), and the other for the gate pulse of the electro-optic (EO) sampling. We combined the two THz pulses to the same optical path using a silicon beam splitter. The transmitted THz pulses from the sample were detected by the EO sampling in a 1-mm-thick ZnTe (110) crystal. The obtained peak THz electric-field ( $E$ -field) strengths for the broad-band A and B pulses are 150 kV/cm and 80 kV/cm, respectively.

For the THz 2DCS experiments, the A-pulse's intensity is attenuated to be equal to that of the B-pulse. Narrow-band THz pulses at the frequency of  $\Omega = 0.63$  THz were generated by placing two bandpass filters in the beam pass of the A-pulse and one filter for the B-pulse. We obtained the peak THz  $E$ -fields of 30 kV/cm for both pulses.

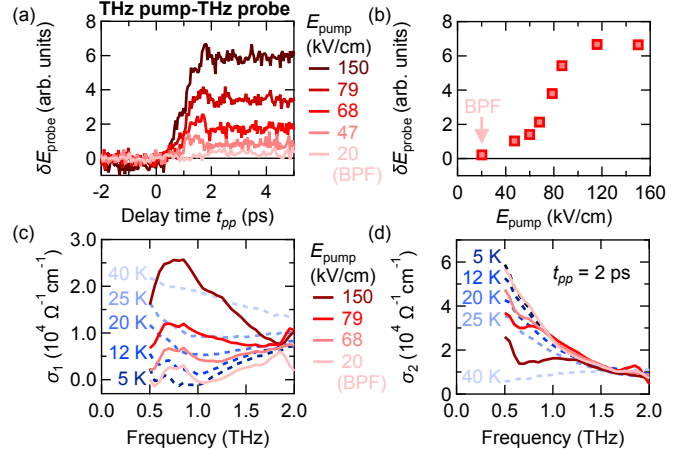


FIG. S3. (a) THz pump-induced change in the THz probe  $E$ -field amplitude ( $\delta E_{\text{probe}}$ ) as a function of the pump-probe delay time  $t_{pp}$  measured at 7 K. The peak THz pump  $E$ -field amplitude is shown in the legend. (b) The maximum value of  $\delta E_{\text{probe}}$  as a function of the pump peak  $E$ -field at 7 K. (c) Real and (d) imaginary parts of the optical conductivity of  $\text{MgB}_2$  at  $t_{pp} = 2$  ps measured at 7 K (solid curves). The dashed curves denote the optical conductivity in equilibrium at selected temperatures.

### IV. THZ PUMP-THZ PROBE EXPERIMENTS

We performed THz pump-THz probe experiments on  $\text{MgB}_2$  at temperatures as low as 7 K to confirm that the SC condensate is not depleted in the THz 2DCS. We employed exactly the same setup of the THz 2DCS, except for a weak broad-band probe THz pulse whose peak  $E$ -field was set to 10 kV/cm. Figure S3(a) shows the THz pump-induced change in the probe amplitude ( $\delta E_{\text{probe}}$ ) as a function of the pump-probe delay time  $t_{pp}$  at the fixed sampling time. With the strongest excitation of 150 kV/cm, we identify a long-lived relaxation of SC quasiparticles. Importantly,  $\delta E_{\text{probe}}$  is almost undetectable for the narrow-band pump with BPF. This is clearly seen by plotting the maximum  $\delta E_{\text{probe}}$  as a function of the pump peak  $E$ -field in Fig. S3(b).

We further evaluated the transient optical conductivity after the THz excitation. Here, we obtained the probe time trace by sweeping the arrival time of the probe pulse while keeping the pump and sampling pulses' time fixed [12, 13]. Figure S3(c) compares the real part of the optical conductivity spectra  $\sigma_1(\omega)$  out of equilibrium at 7 K (the solid curves) and in equilibrium at selected temperatures (the dashed curve). The corresponding imaginary parts  $\sigma_2(\omega)$  are shown in Fig. S3(d). When the pump peak  $E$ -field is set to 150 kV/cm,  $\sigma_1(\omega)$  measured at  $t_{pp} = 2$  ps is close to that at 40 K in equilibrium normal state.  $\sigma_2(\omega)$  is also strongly suppressed but larger than

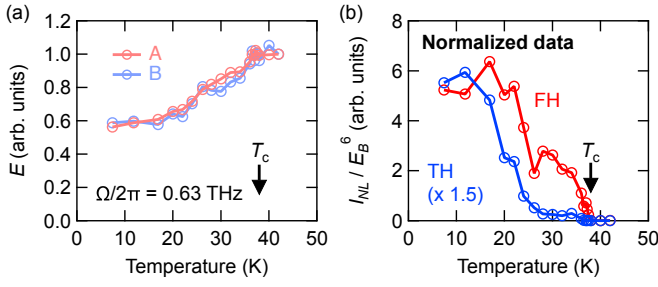


FIG. S4. (a) Transmitted  $E$ -field amplitude at  $\Omega/2\pi = 0.63$  THz of the A and B pulses as a function of temperature. (b) Temperature dependence of the nonlinear signal's intensity for the FH and TH normalized by the sixth power of the B-pulse's amplitude  $E_B^6$ . Here, the field strength of the A and B pulses are set to 12 kV/cm.

that at 40 K. These results indicate that the SC condensate is significantly depleted with the THz peak  $E$ -field of 150 kV/cm. This result clearly demonstrates that the THz pump-probe or 2DCS with THz field stronger or equal to 150 kV/cm is depleting the SC state, and the observed nonlinear signals come from the SC quasiparticle excitation. On the other hand, when the sample is driven by the narrow-band THz pump, both  $\sigma_1(\omega)$  and  $\sigma_2(\omega)$  remain almost intact at  $t_{pp} = 2$  ps. This results ensures that the SC condensate is not depleted in the

current study of THz 2DCS.

## V. NORMALIZATION OF THE NONLINEAR SIGNALS BY MEASURED THZ FIELDS

Figure S4(a) shows the transmitted  $E$ -field strength of the A and B pulses at 0.63 THz as a function of temperature. Due to the temperature-dependent change in the refractive index, the transmitted and internal  $E$ -field decreases when the temperature is lowered. This screening effect must be considered to evaluate the temperature dependence of the third-order nonlinear susceptibility, as documented in Ref. [14]. We normalized the first-harmonic (FH) and third-harmonic (TH) signals by the sixth powers of the  $E$ -field of the A-pulse in Fig. 4 in the main text. While the raw data of the FH signal in Fig. 3(d) for 12 kV/cm displays a resonant enhancement around 35 K where the lower SC gap satisfies  $\Omega = 2\Delta_\pi$ , the normalized FH intensity shows a monotonic increase toward lower temperature. We note that the normalized results do not depend largely on which pulse is used for normalization. Figure S4(b) presents the intensity of the FH and TH signals as a function of temperature normalized by the six powers of the  $E$ -field of the B-pulse, consistent with the results in Fig. 4. These results indicate that the resonant-like enhancement observed in the raw data of the FH intensity is simply due to the temperature-dependent refractive index.

- 
- [1] X. Xi, A. Pogrebnakov, S. Xu, K. Chen, Y. Cui, E. Maertz, C. Zhuang, Q. Li, D. Lamborn, J. Redwing, Z. Liu, A. Soukiassian, D. Schlom, X. Weng, E. Dickey, Y. Chen, W. Tian, X. Pan, S. Cybart, and R. Dynes, *Physica C: Superconductivity* **456**, 22 (2007).
- [2] F. Giorgianni, T. Cea, C. Vicario, C. P. Hauri, W. K. Withanage, X. Xi, and L. Benfatto, *Nat. Phys.* **15**, 341 (2019).
- [3] D. C. Mattis and J. Bardeen, *Phys. Rev.* **111**, 412 (1958).
- [4] W. Zimmermann, E. Brandt, M. Bauer, E. Seider, and L. Genzel, *Physica C: Superconductivity* **183**, 99 (1991).
- [5] J. Fiore, M. Udina, M. Marciani, G. Seibold, and L. Benfatto, *Phys. Rev. B* **106**, 094515 (2022).
- [6] R. A. Kaindl, M. A. Carnahan, J. Orenstein, D. S. Chemla, H. M. Christen, H.-Y. Zhai, M. Paranthaman, and D. H. Lowndes, *Phys. Rev. Lett.* **88**, 027003 (2001).
- [7] S. Kovalev, T. Dong, L.-Y. Shi, C. Reinhofer, T.-Q. Xu, H.-Z. Wang, Y. Wang, Z.-Z. Gan, S. Germanskiy, J.-C. Deinert, I. Ilyakov, P. H. M. van Loosdrecht, D. Wu, N.-L. Wang, J. Demsar, and Z. Wang, *Phys. Rev. B* **104**, L140505 (2021).
- [8] M. Iavarone, G. Karapetrov, A. E. Koshelev, W. K. Kwok, G. W. Crabtree, D. G. Hinks, W. N. Kang, E.-M. Choi, H. J. Kim, H.-J. Kim, and S. I. Lee, *Phys. Rev. Lett.* **89**, 187002 (2002).
- [9] S. A. Kuzmichev, T. E. Kuzmicheva, and S. Tchesnokov, *JETP Letters* **99**, 295 (2014).
- [10] A. Y. Liu, I. Mazin, and J. Kortus, *Physical Review Letters* **87**, 087005 (2001).
- [11] X. Xi, *Reports on Progress in Physics* **71**, 116501 (2008).
- [12] K. Isoyama, N. Yoshikawa, K. Katsumi, J. Wong, N. Shikama, Y. Sakishita, F. Nabeshima, A. Maeda, and R. Shimano, *Commun. Phys.* **4**, 160 (2021).
- [13] K. Katsumi, M. Nishida, S. Kaiser, S. Miyasaka, S. Tajima, and R. Shimano, *Phys. Rev. B* **107**, 214506 (2023).
- [14] K. Katsumi, J. Fiore, M. Udina, R. Romero, D. Barbalas, J. Jesudasan, P. Raychaudhuri, G. Seibold, L. Benfatto, and N. P. Armitage, *Phys. Rev. Lett.* **132**, 256903 (2024).